

Picking first arrivals in hydroacoustic seismograms from MERMAID floats

Guust Nolet  ^{1,2}, Nguyen Ba Hoang  ³, Sébastien Bonnieux  ², Yuko Kondo  ⁴, Fanchao Kong  ⁵, Masayuki Obayashi  ⁶, Sirawich Pipatprathanporn  ², Karin Sigloch  ¹, Joel D. Simon  ², Frederik J. Simons  ², Hiroko Sugioka  ⁴, Junko Yoshimitsu  ⁶, Qinglin Zhang 

¹Université de la Côte d'Azur/CNRS/OCA/IRD, Géoazur, Sophia Antipolis, 06560, France, ²Department of Geosciences, Princeton University, Princeton, NJ 08544, USA., ³University of Science and Technology, Danang, Vietnam, ⁴Kobe University, Kobe, Japan, ⁵Southern University of Science and Technology, Shenzhen, China, ⁶Research Institute for Marine Geodynamics, JAMSTEC, Yokosuka 237-0061, Japan

Author contributions: *Conceptualization:* Guust Nolet, Joel Simon, Frederik Simons. *Methodology:* Guust Nolet. *Software:* Guust Nolet, Sébastien Bonnieux, Joel Simon. *Formal Analysis:* All authors. *Writing - Original draft:* Guust Nolet. *Writing - Review & Editing:* All authors.

Abstract Floating seismometers ('MERMAIDs') operating in the noisy environment of the world's oceans pose a challenge for picking the time of earthquake first arrivals. We report on an experiment to estimate the errors in picked arrivals from 49 MERMAIDs operating in the South Pacific, using two independent strategies. For 15 events, the same arrivals were redundantly picked by several analysts, allowing for a direct estimate of error distributions. Standard errors in times from MERMAID seismograms vary from 0.2 s for close events at mantle depths in the Kermadec subduction zone to more than 2 s for crustal events at large epicentral distance. In a second experiment, we analysed the a posteriori misfits after tomographically inverting all events. The residual traveltimes misfit is consistent with the error estimates from the first experiment, but also shows inconsistencies with arrival times from the ISC-EHB and NEIC catalogues, which we attribute to errors in the published hypocentres and/or origin times.

Non-technical summary To locate earthquakes, or to investigate the Earth's interior using tomographic methods, one observes (or 'picks') the time of arrival of seismic waves. We investigate the accuracy of such picks if the seismograms originate from autonomous robots (MERMAIDs) that float at depth in the oceans. Such data are generally much noisier than those from seismographs on land. We find that arrivals from earthquakes below the crust can often be picked with uncertainties as small as 0.2 s, but those in the crust, or weaker signals from larger distance have errors as large as 2 s. We also found that earthquake locations and origin times as determined from land stations may need correction when confronted with the new type of data provided by MERMAIDs.

Production Editor:
Andrea Llenos
Handling Editor:
Lise Retailleau
Copy & Layout Editor:
Anna Ledeczi

Signed reviewer(s):
Sara Bazin

Received:
17 November 2024
Accepted:
9 April 2025
Published:
25 April 2025

1 Introduction

MERMAIDs or 'Mobile Earthquake Recording in Marine Areas by Independent Divers' (Simons et al., 2009) drift passively deep below the ocean's surface (typically at 1500 m) and are equipped with a continuously recording hydrophone. The passband of the instrument is between about 0.05 Hz to the Nyquist frequency of 10 Hz, though only local events generate significant signal above 2 Hz. A triggering algorithm (Sukhovich et al., 2011) keeps track of presumed P-wave arrivals. For sufficiently strong signals, it commands the float to rise to the surface, transmit the most recent recording with a latency of several hours, depending on the rise time, together with possible weaker P-arrivals stored earlier. The location where the actual recording took place is determined by interpolation of GPS fixes (Nolet et al., 2024).

The noise level in the seismograms is generally high, rendering the picking of first arrivals difficult. We have developed a first-arrival picking strategy based on comparison with other MERMAIDs and nearby island stations, knowledge of the expected polarity of the P-

wave, and using both broad-band and high-pass filtered records. The data processing of the MERMAID seismograms includes an initial arrival time estimate using the Akaike Information Criterion, or AIC (Simon et al., 2020) which is often—but not always—within about 0.2 s of the visual pick by the analyst. Since MERMAIDs are relatively recent additions to the seismological toolbox, not enough data are yet available to train an AI-based algorithm (Mousavi et al., 2019; Lomax et al., 2024), though we hope that the current effort will take us many steps in that direction.

The data in this study are from 49 MERMAIDs in the South Pacific, of which the earliest were launched in June 2018 as part of the SPPIM, or 'South Pacific Plume Imaging and Modeling', project (Simon et al., 2020, 2021). The large majority of floats are still operational today and in this paper we use data transmitted until November 2023. A live map of the state of the network is available on the web (www.earthscopeoceans.org), where one can also inspect the history of each float. All data are being archived by the EarthScope Consortium with FDSN network code MH.

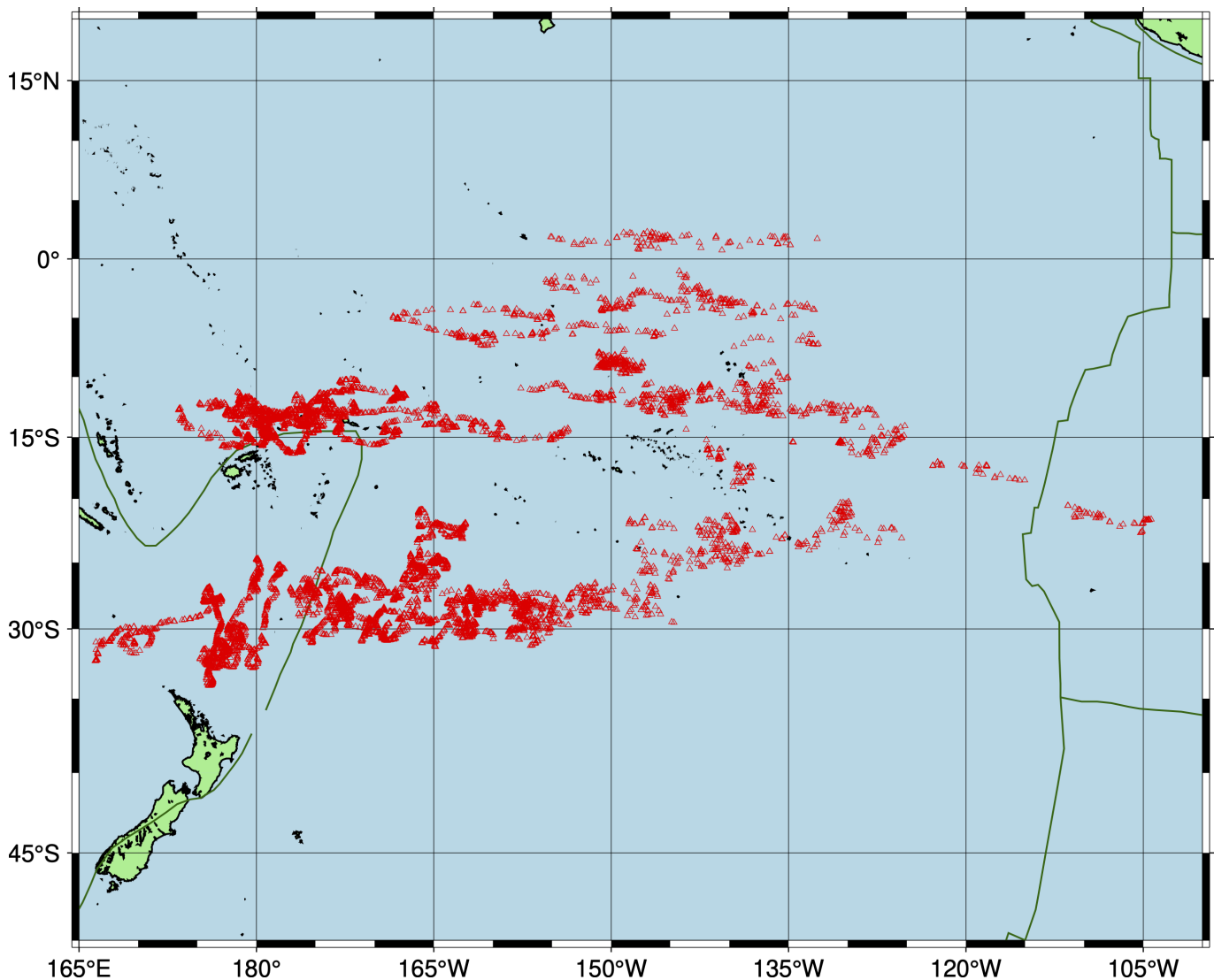


Figure 1 Locations where MERMAIDs recorded the seismograms used in this study. Note the increased density in the western part of the domain, where many very weak Tonga-Fiji and Kermadec events occurred close enough to the instruments to have an acceptable signal-to-noise ratio. Plate boundaries are indicated by thin black lines.

Our team of ‘pickers’ consists of experienced seismologists, PhD students and postdocs from institutions participating in SPPIM (see author list). Prior to doing the experiment, a series of training sessions was held via Zoom, of which the materials are available on the web for future users of MERMAIDs (Nolet, 2024). Since the ultimate goal of SPPIM is to sharpen tomographic images of the upwelling mantle structure(s) beneath the South Pacific, a correct estimate of picking errors is essential.

Ideally, we would like to see picking errors well below the uncertainty introduced by the crustal corrections in tomography and possible errors in the location of the float. In our case, the error in crustal corrections is dominated by the uncertainty in satellite bathymetry, which cannot account for rapid changes at wavelengths < 10 km. Sepúlveda et al. (2020) give an estimated standard error of 160 m for satellite bathymetry near Chile. Our own knowledge of bathymetry errors is largely anecdotal, but it has not been unusual to see a MERMAID float happily at 1500 m where the bathymetry from GEBCO 2014 (Weatherall et al., 2015) reports less

than a one kilometre of water depth, indicating the error may be significantly larger than 160 m in the SPPIM area. We must add to this the error in the corrections for the Moho depth and oceanic crustal structure, for which we used the crustal part of LITH1.0 (Pasyanos et al., 2014). We therefore assume a prior uncertainty in the total crustal correction of 0.4 s in tomographic inversions.

The equivalent travel time delay error caused by mislocation of the float is generally below 0.1 s (Nolet et al., 2024). Contrary to OBS data, we do not have to worry about clock correction errors (Naranjo et al., 2024) since the internal clock drift is regularly measured, and corrected for, by GPS at each surfacing.

To estimate the picking errors we develop two strategies. In the first experiment, seismograms from MERMAIDs as well as nearby island stations are picked multiple times by different pickers. In the second experiment, we invert the 16,739 arrival time picks from 1850 events and measure the a posteriori fit to the predicted times.

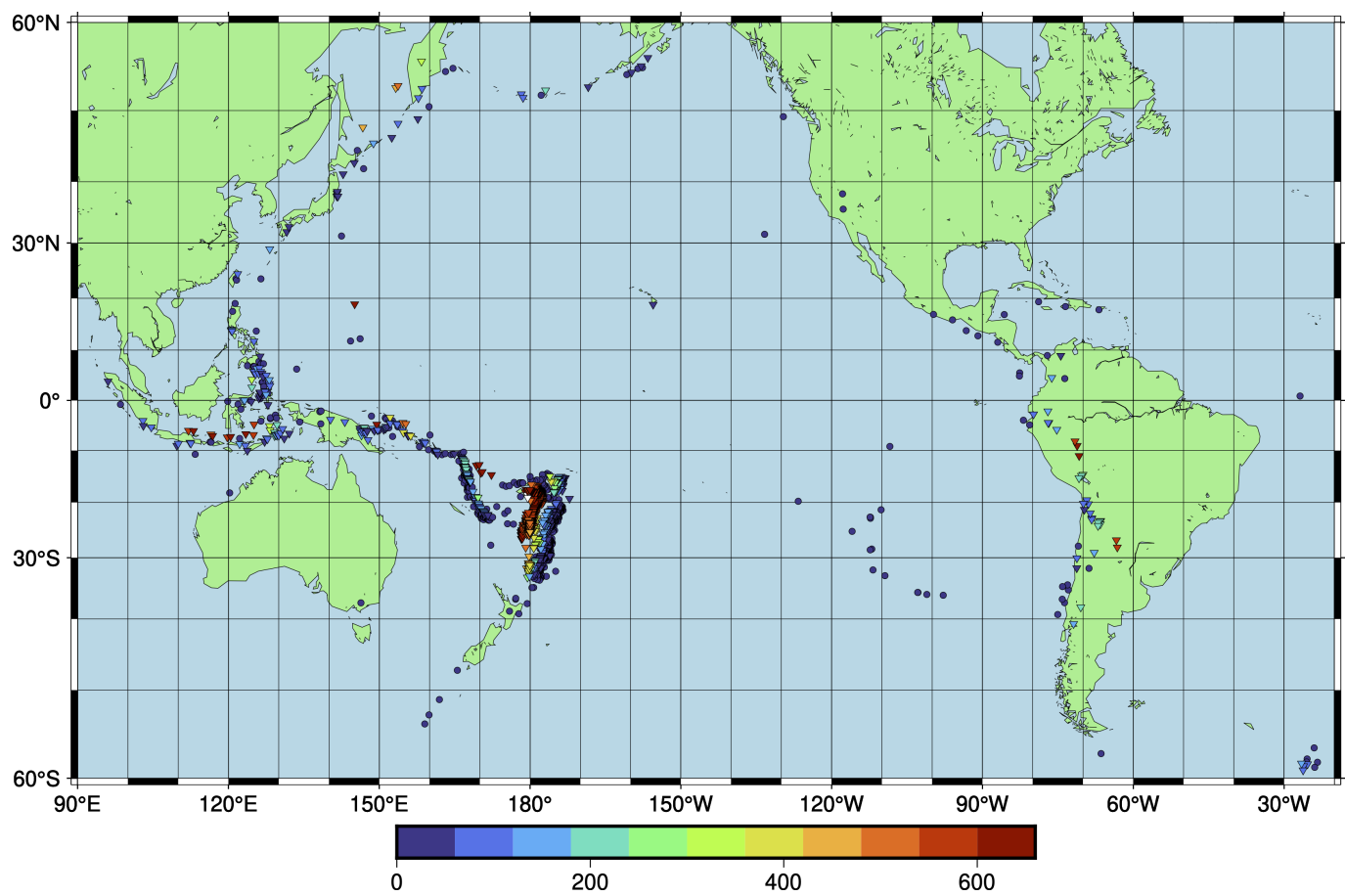


Figure 2 Locations of 1147 deep events (triangles) and 703 shallow ones ($h < 35$ km, circles) analysed in Experiment 2, with colour indicating the hypocentre depth in km.

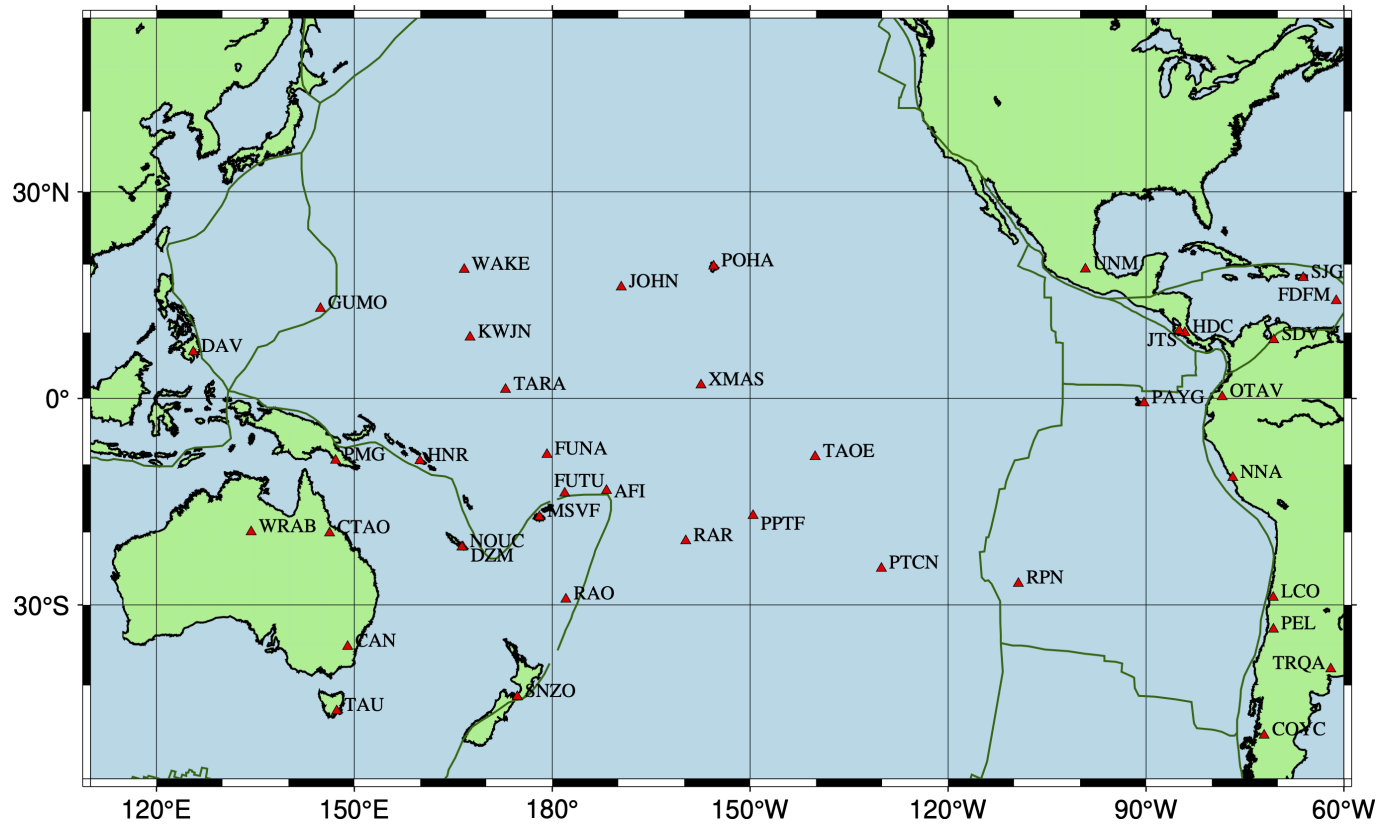


Figure 3 Locations of the 40 surface (land) stations used to compare waveforms.

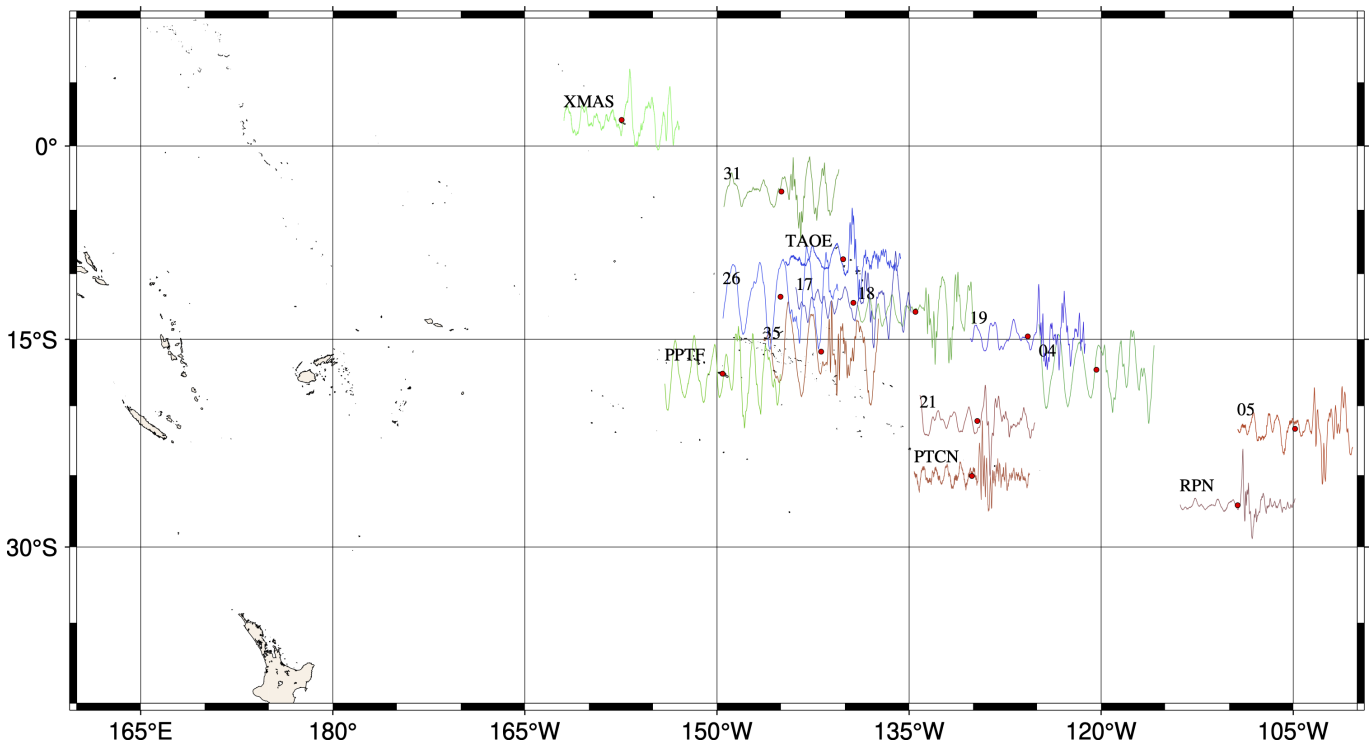


Figure 4 All MERMAID seismograms picked for the M 6.5 event of 2022/06/08 in the Peru-Brazil border region plotted on a map and identified by number, together with nearby surface stations. The red dot indicates the station location, and is also the expected time of arrival of the P wave for model AK135. The seismograms are plotted in different colours to increase visibility where they overlap. Each trace has a length of 30 s and is scaled to equalize the maximum amplitude.

2 Data

The 49 MERMAIDs in the SPPIM project were launched from scientific vessels operated by Ifremer in France and JAMSTEC in Japan. The first float (P0006) was launched on June 26, 2018. Two more cruises followed until the network was complete by September 2019. At the time of writing this paper in the Fall of 2024 all floats had thus exceeded their designed battery lifetime of 5 years, and 36 of them were still operating, including P0006, which attests to the durability of the instrument. Figure 1 shows the locations where MERMAIDs recorded a seismogram from one of the earthquakes shown in Figure 2. We used 40 surface (or borehole) stations from the Global Seismic Network (GSN) to compare waveforms (Figure 3). Arrivals at these stations are picked as well, such that we are able to compare the quality of picks from surface stations with those from the MERMAIDs. In total, we assembled 5,384 picks from MERMAIDs and 11,355 from surface stations. The addition of land station picks is also done to be able to apply event relocations and origin time corrections at the time of inversion, since the number of MERMAID picks can be very limited for low magnitude events only recorded by nearby floats. For all events, hypocentre metadata are taken from the ISC-EHB catalogue when available (i.e. until 2020). For more recent events we use the latest NEIC estimates.

We have developed a highly streamlined procedure to pick first arrivals, implemented as Linux shell scripts. Figures 4 – 6 show the diagnostic screen output an analyst is presented with prior to picking an event. All

seismograms for the event are plotted on a map to enable visual comparison in geographical context (Figure 4), as well as combined in one plot in an order that allows for easy comparison of nearby stations (Figure 5). The most useful plot is that of the predicted polarity (Figure 6), using published moment tensor estimates. Whenever available (which is for about 7% of the events), we use the SCARDEC double-couple tensor (Vallée et al., 2011). Since SCARDEC uses only the P wave-train, whereas CMT solutions are based on long periods (> 45 s) and include surface waves (Ekström et al., 2012; Rösler et al., 2023, 2024), SCARDEC is more representative for the high-frequency arrivals that we target than published centroid moment tensor (CMT) estimates. In any case, we inspect the plot for any systematic deviations from the predicted polarity—which occur especially near the (white) nodal zones. Unless the prediction is ambiguous, we only pick an arrival that has the predicted polarity as read from this plot. Finally, we also inspect SCARDEC source time functions (Vallée and Douet, 2016), whenever available.

Once this initial orientation complete, the Seismic Analysis Code (SAC) program (Goldstein et al., 2003; Goldstein and Snook, 2005) is called up and seismograms are shown one after the other in a sequence that tries to optimize nearby seismograms following each other. Figure 7 shows an example of such plot, offering the seismogram both as a record high-passed at 1 Hz (using a one-pass Butterworth filter with only two poles, which produces a rather gentle damping of lower frequency), and as the original broadband record. To help identify the P-arrival in the presence of noise, the

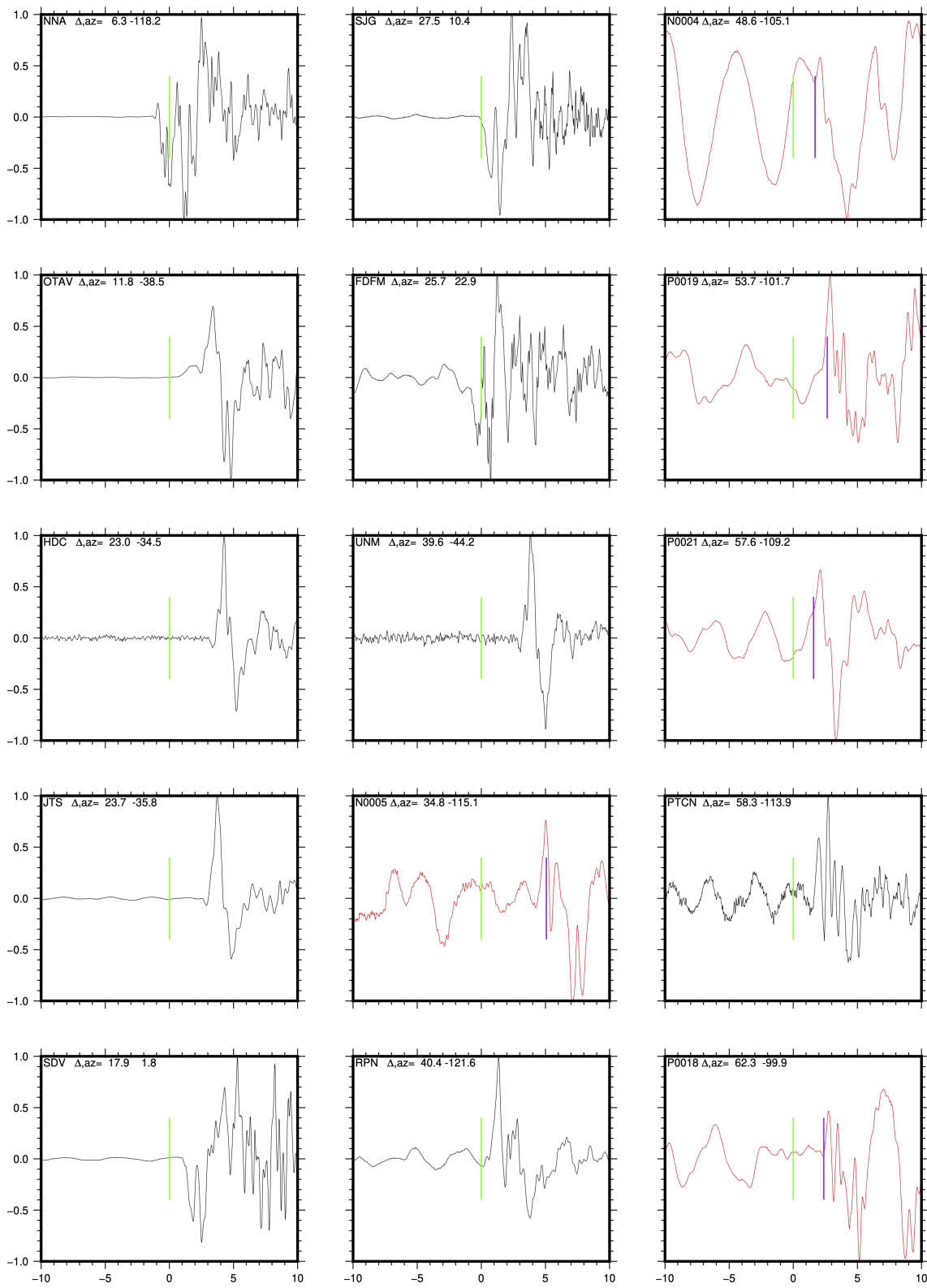


Figure 5 Seismograms for the event of 2022/06/08 plotted in an order that allows for easy comparison of waveforms at nearby stations. Epicentral distance Δ and azimuth are plotted in the upper left corner. The green line indicates the expected P wave arrival (using model AK135), purple lines those of the AIC pick from [Simon et al. \(2020\)](#) in MERMAID seismograms. To distinguish them from surface stations, MERMAID seismograms are coloured red.

arrival time predicted by the radially stratified model AK135 (“P”) and the AIC estimate of the arrival (“F”) are superimposed as vertical lines. The latter detects where the variance of the time series changes in the 1–5 Hz frequency band, essentially showing where the frequency content of the seismogram changes apprecia-

bly. Though the MERMAIDs record and store data with a 40 Hz sampling frequency, transmission is normally done at 20 Hz to save transmission time and cost, which has proven sufficient for accurate picking.

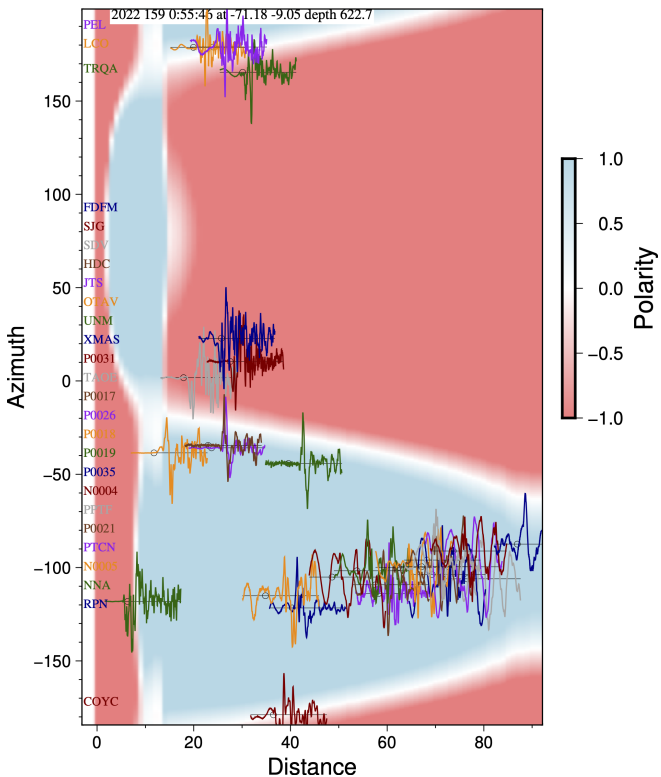


Figure 6 Predicted polarity (UP=blue) for event 2022/06/08 (71°W, 9°S, 622 km depth). Small circles indicate distance and azimuth, plotted at the expected arrival time of the P wave. Many overlapping seismograms are hard to distinguish even when plotted in different colours, but are nevertheless shown, simply to indicate the coverage of MERMAIDs and island records in the distance/azimuth plane.

3 Experiment 1: Picking by analysts

Picking for both experiments is done for clusters of closely located events, arranged in order of decreasing magnitude. This allows for the analysts to get used to the peculiarities of data coming from certain regions while learning to pick data with a high signal-to-noise ratio before continuing on to lower magnitudes. Only events with at least one MERMAID pick are included in our data set. For the duplicate picks of experiment 1 we select six clusters of events listed in Table 1.

Each event is picked by up to 12 analysts. For each event, we calculate the average pick time for each station as well as the deviation Δt for each pick. The distribution of these residuals Δt is used as a proxy for the picking errors. For each of the six clusters we compute the RSDR or Robust Standard Deviation of the Residuals (Motulsky and Brown, 2006), which essentially defines the 68% confidence limit. A first RSDR estimate was used to remove a few (26) outliers beyond 3 standard deviations before computing the final RSDR again.

For the three deep clusters A, B, and C, MERMAID residuals are in an acceptable range (Table 2). The fact that the RSDR for the events in the magnitude 4 range (cluster C) is smaller than that for magnitude 5 (cluster B) can probably be explained by the fact that, even though the amplitude is smaller, the frequency of the

Table 1 Events used in Experiment 1. The last three columns list the magnitude M (which is the moment magnitude M_w when available), the number of picks from MERMAID hydrophones (N_{MH}), and those from surface station seismometers (N_{GSN}).

Date	Lat (deg)	Long (deg)	Depth (km)	M	N_{MH}	N_{GSN}
Cluster A						
2018/08/24	-11.035	-70.781	618.2	7.1	25	211
2019/01/05	-8.165	-71.587	580.0	6.8	72	146
2022/06/08	-9.047	-71.178	622.7	6.5	124	222
Cluster B						
2018/10/07	-28.194	-179.196	400.0	5.6	36	203
2018/11/29	-27.361	-178.061	256.5	5.1	9	111
2021/09/22	-27.556	-178.810	352.5	5.0	70	111
Cluster C						
2023/02/09	-26.649	-178.300	263.8	4.9	73	44
2020/11/22	-28.334	-179.274	396.9	4.5	24	44
2022/09/20	-27.760	-178.995	356.9	4.5	34	48
2020/02/12	-26.754	-178.361	320.5	4.1	13	27
2020/11/15	-26.568	-178.157	233.3	4.1	6	40
2019/09/01	-27.241	-178.368	322.8	4.0	5	1
Cluster D						
2020/01/28	19.350	-78.847	10.0	7.7	88	89
2021/08/14	18.434	-73.482	10.0	7.2	47	194
2020/01/07	17.824	-66.823	13.7	6.4	18	108
Cluster E						
2022/11/22	-9.820	159.603	14.0	7.0	127	183
2022/11/22	-9.820	159.459	10.0	6.0	87	151
2021/10/15	-8.878	158.464	33.0	6.4	17	69
Cluster F						
2020/03/14	-27.695	-175.697	15.0	6.4	108	217
2021/08/14	-22.421	-174.552	10.0	5.6	44	86
2021/06/26	-28.330	-176.549	10.0	5.3	63	39
2021/04/16	-30.414	-177.766	10.0	5.0	22	39
2021/06/03	-24.984	-175.696	10.0	4.8	32	7
2021/04/17	-27.192	-175.923	10.0	4.4	28	11

P wave from weaker events is higher. Also, such weak events are only observed at close or regional distances, again favouring a higher frequency, which is easier to pick.

But the failure of MERMAID picks for shallow events in clusters D and E to match the precision of those from surface stations is disappointing. Whereas the RSDR for the three deep clusters gives a distribution of Δt that is comparable between MERMAIDs and surface stations, the shallow events are picked with a rather erratic distribution of residuals, in contrast to that for the land stations (Figure 8). The exception is cluster F, which has shallow events close to the network of MERMAIDs, resulting in easily observable high frequency onsets.

The overlap in frequency of seismic noise and that of P waves from shallow earthquakes is large, making the identification of an onset more difficult. The histograms of MERMAID picks for shallow clusters D and E show a distribution that is clearly not Gaussian, and dominated by many delays in excess of the RSDR shown in Table 2. Those in the Caribbean (cluster D) with an RSDR of 2.5 s are essentially useless for seismic delay-time tomography, where the useful signals, i.e. traveltime delays introduced by velocity heterogeneities, are generally smaller. Recent efforts in waveform fitting of MER-

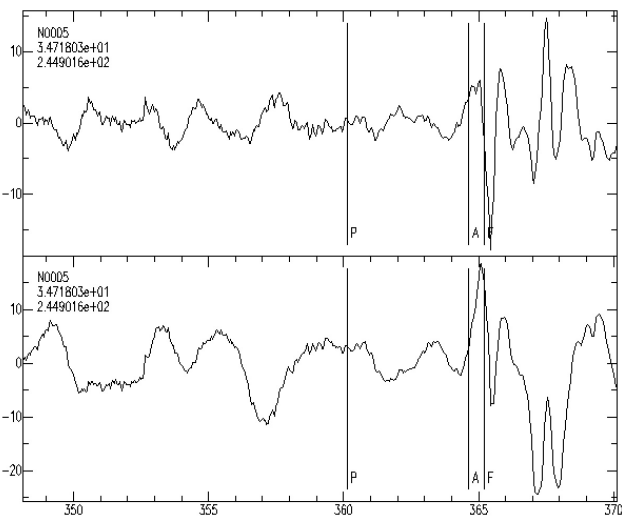


Figure 7 SAC plot used for picking of the seismogram of 2022/06/08 recorded by MERMAID N0005. The original seismogram is at the bottom, a high-passed version (corner frequency 1 Hz) is at the top. The line marked by P is the AK135 (Kennett et al., 1995) predicted arrival, F the AIC pick, and A the visually picked first arrival. Arrivals can be picked on either of the two plots.

Table 2 RSDR of pick distributions (s)

Cluster	Region	σ_{MH}	σ_{GSN}
Cluster A	Peru-Brazil	0.27	0.10
Cluster B	Kermadec Isl.	0.48	0.24
Cluster C	Kermadec Isl.	0.20	0.19
Cluster D	S. of Tonga	2.50	0.40
Cluster E	Solomon Isl.	1.33	0.66
Cluster F	S. of Tonga	0.39	0.29

MAID seismograms by Pipatprathanporn and Simons (2024) have been successful and should significantly reduce misidentification of pP as P, which we have observed in some of our picks and suspect to be a main cause of outliers.

4 Experiment 2: Insights from tomographic analysis

The analysis in the previous section was straightforward, since it was directly done on multiple measures of the same source-receiver path. In the second experiment we seek to confirm the findings of experiment 1 by using the interdependence of the data, as provided by the linearized tomographic equations, e.g. Nolet (2008):

$$Am = d, \quad (1)$$

where m is a vector of model parameters (which may include source corrections), and d are the data, scaled to unit variance. The delays d vary because the paths through the 3D Earth differ, but also because of picking errors. Whereas the delay caused by the velocity anomalies m of the Earth induces a correlation between the observed travel times because of (1), its errors are in principle uncorrelated between different source-

Table 3 Distribution of P wave picks among MERMAIDS and global network stations

	Number of events	Total picks	MER-MAID	(is)land stations
deep (>35 km)	1147	11222	3552	7670
shallow	703	5517	1832	3685

station paths. The total picked data set available consists of 16,739 picks. Their distribution among shallow and deep events is shown in Table 3.

Voronin et al. (2014) project the delay time observations onto the nullspace of the matrix AA^T to annihilate the influence of the Earth's structure. If U diagonalizes AA^T then the distribution of the projected delays $\tau = U^T d$ approaches the error distribution with variance σ_e^2 as the eigenvalue $\lambda_i \rightarrow 0$ since its variance satisfies:

$$\sigma_{\tau_i}^2 = \lambda_i^2 \sigma_m^2 + \sigma_e^2, \quad (2)$$

where σ_m^2 is the variance in delays caused by heterogeneities in the Earth. If $\lambda_i = 1$, the signal-to-noise ratio of projected delay τ_i is 1, but if $\lambda_i = 0$, τ_i is fully in the nullspace of A and has variance σ_e^2 . Nolet and van der Lee (2022) split data into event clusters so as to reduce the size of A for each cluster while optimizing the overlap of rays (and thus the dependence of rows of A) to obtain a large nullspace and estimate the standard errors in the ISC-EHB catalogue of delay times.

We tried initially to do this also for the picks in MERMAIDS and island stations, only to find that no eigenvalue was smaller than 0.1, even for clusters of closely spaced events, reflecting a high independence between these data caused by the fact that the floats move around and few raypaths are therefore duplicated. Figure 9 shows the distribution of projected data τ_i as a function of eigenvalue λ_i for the most densely packed cluster of shallow earthquakes. Whereas one clearly observes the variance decreasing with λ_i as predicted by (2), there is no way we can reliably estimate σ_e from the left part of the plot: there are few or no λ_i of magnitudes $\ll 1$ for which σ_m can be ignored in (2) to estimate the variance of τ independent of model influence. While the absence of small λ_i is good news for any tomographic inversion, for our experiment it means that the best we can do is establish some lower bound for the picking errors by investigating the a posteriori misfit to the observed traveltimes to those predicted by the tomographic model (Am), after imposing a reasonable regularization on m to force (1) to be overdetermined.

To avoid that the model parametrization introduces limitations in the resolution that contribute to the misfit we must use a very fine grid of model voxels. We use the cubic Earth parametrization of Charléty et al. (2013) which has 3,637,248 voxels to model crust and mantle. The average voxel size is 72 km at the surface and 66 km at the bottom of the upper mantle. Voxel thickness is adapted to fit major discontinuities but is 78 km on average. Regularization is done by penalizing a sum of $|m|$ and $|\nabla^2 m|$ with m weighted by prior uncertainty—see Nolet (2008). For the velocity anomaly δV_P we used a prior model parameter uncertainty of 1%. When addi-

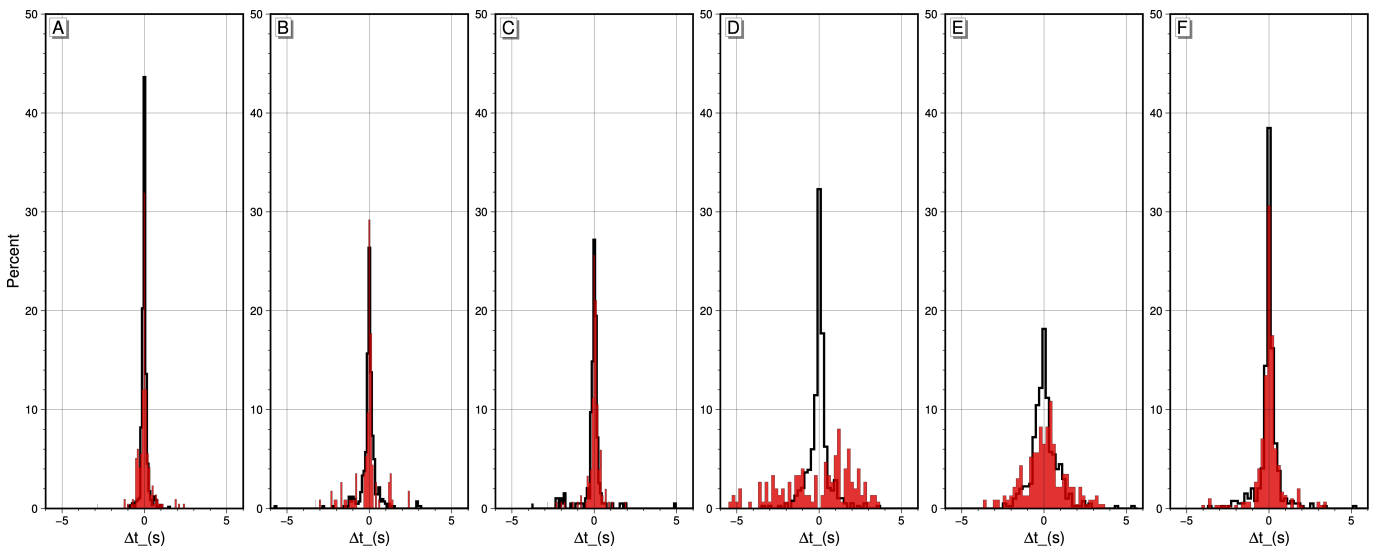


Figure 8 Distribution of Δt for shallow events of clusters A–F observed in surface stations (thick black line) and MERMAIDS (red histogram) shows the irregular distribution of MERMAID picks for cluster D.

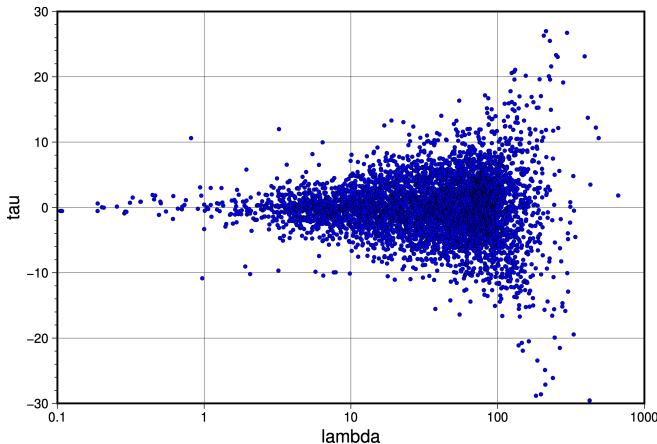


Figure 9 Projected data τ_i as a function of eigenvalue λ_i for the most densely packed cluster of shallow earthquakes (in Tonga-Fiji). Note the paucity of small λ_i , indicating a high relative resolution for this subset of data.

tionally including source corrections we used a prior parameter uncertainty δT_0 of 1 s for the origin time, and 20 km for the uncertainty δh in depth, longitude and latitude. Weston et al. (2018) give an average bias of 11 km for the ISC-EHB hypocentres, but the bias in subduction zones—where many of the earthquakes in this study are located—is known to be much larger (Herrin and Taggart, 1968). Regularization limits how much of the data error can ‘creep’ into the model solution to reduce the a posteriori misfit, but cannot exclude the possibility that at least some of the data may have been erroneously over-fitted by m . The a posteriori misfit for N univariant travelttime data defined as $\chi^2/N = |d - Am|^2/N$ therefore only provides a lower bound for the actual data errors. As in experiment 1, we removed outliers with a misfit beyond 3σ after an initial, only slightly damped inversion, before calculating a final χ^2/N estimate (our tomography code computes the standard deviation σ of the misfit in the classic way, which approaches the more robust RSDR as the distribution approaches the Gaus-

sian).

Since there is ample freedom to choose the regularization, we present six tests, summarized in Table 4. Whereas the results of Experiment 1 are independent of any errors in the hypocentre or origin time, the misfits in the inversion are influenced by errors in source parameters. This can be dealt with by allowing ‘source corrections’ to be part of the modeling. The first three (A–C) are done with (1) including corrections for the origin time and the hypocentre. These corrections are omitted in the last three tests (D–F), as indicated by zero prior uncertainties δT_0 and δh in the table. Since source corrections require a decent azimuthal coverage of the observations, which is often insufficient when only GSN island stations are picked, we supplement our picks with a selection of data from the ISC catalog (until 2020) and NEIC (after 2020). We divide the source azimuth into six sectors of 60° and require the combined data set to have at least four azimuth sectors with two or more data. A small number of events not satisfying that criterion were rejected for these tests. The added travelttime picks from the catalogs are chosen as closely as possible to the source and such that the azimuths are as evenly distributed as possible. Results are shown in Table 4 and Figure 10.

We monitor the model norm so that we can diagnose instabilities caused by data errors. However, the root mean squared (RMS) norm of the global model m is not very useful since we are focusing on the South Pacific. Therefore, as an indication of the model values, the table lists two proxies for the model norm: δV_p^{loc} is a local average $d \ln V_p$ in percent found between $178\text{--}180^\circ\text{E}$, $30\text{--}32^\circ\text{S}$ at a depth of 68 km (the location of a large negative anomaly), and δV_p^{max} is the largest (absolute) anomaly in percent found throughout the whole model. For tests A–C our δV_p^{loc} is close to the anomaly of -5.1% found in this region in model UU-P07 (Amaru, 2007; Hall and Spakman, 2015). The depth where this maximum is found is listed in the next column.

Test A, with only our own picks, serves to check on the internal consistency of the picks. We damp to get

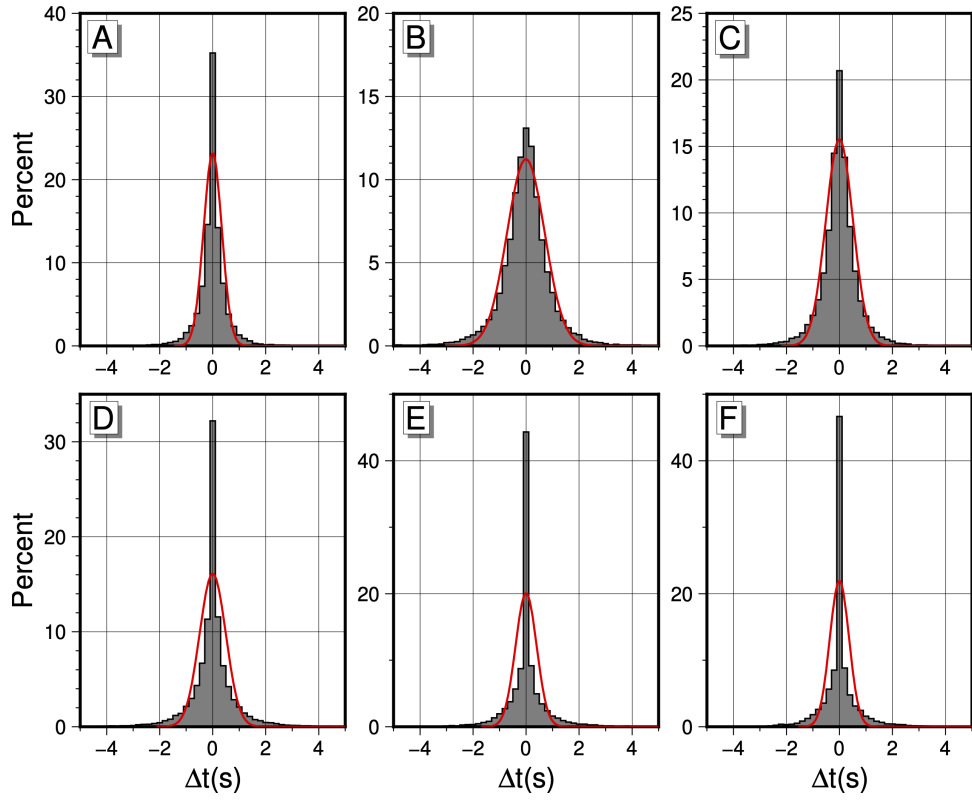


Figure 10 Histograms of the a posteriori fit of delay times for Tests A-F. The red line shows a Gaussian distribution with the RSDR as standard deviation.

Table 4 Results of inverting (1) with different regularizations.

Test	δT_0 (s)	δh (km)	data	χ^2/N	δV_p^{loc} (%)	outliers (%)	δV_p^{max} (%)	depth (km)	RSDR (s)
A	1	20	picks only	1.05	-6.1	0.1	10.6	68	0.34
B	1	20	picks + cat	1.82	-5.6	0.8	9.3	34	0.71
C	1	20	picks + cat	1.01	-6.8	0.8	15.3	68	0.51
D	0	0	picks + cat	1.00	-8.5	2.7	469.8	2869	0.50
E	0	0	picks only	1.19	-10.4	3.3	101.6	11	0.38
F	0	0	picks only	1.04	-11.0	3.3	116.7	11	0.36

an overall misfit $\chi^2/N \approx 1$, which gives an RMS misfit of 0.63 s, close to the prior error of 0.57 s assigned to most picks, as expected. However, the RMS estimate is heavily influenced by outliers. The RSDR, which is stable in the presence of outliers, is 0.34 s and of the same order of magnitude as the standard deviations found in experiment 1 for deep events, but lower than for the shallow ones. Since the inversion mixes both deep and shallow events, this indicates that some of the errors are being fitted by the model, but it does not invalidate the results of experiment 1 (it would only if the RSDR exceeded those errors). The values for the model norm proxies are acceptable for a tectonically active region. For example, model UU-P07 has δV_p range between -9.5% in Hokkaido near the surface, to +9.9% in the Tonga subducting slab.

In test B we add the catalogue data to better constrain the event corrections, but leave the damping unchanged. As a result χ^2/N is not close to 1 (it is 1.82), which could still be acceptable if our error estimates are in error by about 35% ($\sqrt{1.82} = 1.35$). The RSDR more than doubles to 0.71 s (the RMS estimate was 1.05 s). This is still consistent with experiment 1, but it does indicate an incompatibility between catalogue data and our picks. One explanation for the increased RSDR is that catalogue data have originally been fitted with a source in the wrong location, which became incompatible after adding MERMAID data to complete the azimuthal coverage. There may also be a difference in the quality for catalogue picks that were possibly obtained by an algorithm without human intervention (according to their web site, the ISC analysts review about 10-20% of the events in their data base). In the case of island station picks, there are a few duplications of catalogue data with our picks. We visually checked several of the largest discrepancies and are confident that with few exceptions our picks are accurate.

In test C we relax the damping to obtain $\chi^2/N = 1.01$, which lowers the RSDR to 0.51 s, but raises δV_p^{max} to 15.3%, a clear indication that model variations are trying to compensate for inadequate source corrections.

To further investigate the role of the hypocentre in the a posteriori misfit, we eliminate the source corrections in tests D-F. The source location and time are thus tailored to the catalogue data and ignore the new information from MERMAIDs. Inverting the combined data set (test D) while reducing the damping such that $\chi^2/N \approx 1$ results in a severe instability, with the model parameters exceeding 100% outside the region of interest. Using the same damping as in (A) for picks only, still gives unacceptably large δV_p^{max} (test E). We conclude that source corrections are absolutely necessary, since in this case the model velocity anomalies are trying to compensate for the absence of source corrections. Changing the damping to obtain a fit near 1 does not change that conclusion (test F).

5 Conclusions

Even though MERMAIDs operate in a noisy oceanic environment, the onset of P waves can be picked with an accuracy well below 0.5 s if the earthquake is located

below the crust. For crustal earthquakes the accuracy varies strongly with the frequency content of the P wave. Discrepancies show up when our arrival times are inverted together with those published in catalogue data, which points to the significance of event mislocations in oceanic areas. Such mislocations can be avoided by employing MERMAIDs in oceanic areas of interest, such that the azimuthal coverage is improved. The source corrections themselves are obviously of interest, and since the dominant drift of the floats is westwards, more data on them are steadily accumulating. We shall study them in a follow-up paper.

Acknowledgements

We thank Carlos Becerril for his assistance with experiment 1. MERMAIDS were developed as part of ERC project GlobalSeis (advanced grant 226837). Ifremer (France) and JAMSTEC (Japan) provided the ship-time for launching SPPIM floats (doi:10.17600/18000882, doi:10.17600/18000519 and doi:10.17596/0002686). J. D. S. was supported by National Science Foundation (NSF) Grant Numbers OCE-1917058 and EAR-2341811 to Frederik J. Simons and Jessica C.E. Irving. The Japanese contribution to SPPIM, including 9 MERMAIDs, was financed through JSPS KAKENHI Grant 19H00731. K.S. was supported by the UCAJEDI Investments in the Future project (reference ANR-15-IDEX-01). Princeton financed 16, and SUSTech financed 23 of the MERMAID floats. We used GMT6 for plotting (Wessel et al., 2019).

Data and code availability

The MERMAID metadata and seismograms are available at the EarthScope Consortium data center (<https://www.earthscope.org/>; formerly Incorporated Research Institutions for Seismology [IRIS]) under the network code "MH" (doi: 10.7914/SN/MH). With a few exceptions (P0006, P0007, P0008, P0010, and P0016) these seismograms are embargoed for two years after acquisition. ISC-EHB data (Weston et al., 2018; Engdahl et al., 2020; International Seismological Centre, 2020) are available from <http://www.isc.ac.uk/isc-ehb/>, and NEIC arrival times from <https://www.sciencebase.gov/catalog/item/5d110ca0e4b0941bde550412> All websites were last accessed on Nov 8, 2024.

Competing interests

The authors have no competing interests.

References

- Amaru, M. L. *Global Travel Time Tomography with 3-D Reference Models*. PhD thesis, Utrecht University, 2007.
- Charléty, J., Voronin, S., Nolet, G., Loris, I., Simons, F. J., Sigloch, K., and Daubechies, I. C. Global seismic tomography with sparsity constraints: Comparison with smoothing and damping regularization. *Journal of Geophysical Research: Solid Earth*, 118 (9):4887–4899, Sept. 2013. doi: 10.1002/jgrb.50326.

Ekström, G., Nettles, M., and Dziewoński, A. The global CMT project 2004–2010: Centroid-moment tensors for 13,017 earthquakes. *Physics of the Earth and Planetary Interiors*, 200–201:1–9, June 2012. doi: [10.1016/j.pepi.2012.04.002](https://doi.org/10.1016/j.pepi.2012.04.002).

Engdahl, E. R., Di Giacomo, D., Sakarya, B., Gkarlaouni, C. G., Harris, J., and Storchak, D. A. ISC-EHB 1964–2016, an improved data set for studies of earth structure and global seismicity. *Earth and Space Science*, 7(1):e2019EA000897, Jan. 2020. doi: [10.1029/2019EA000897](https://doi.org/10.1029/2019EA000897).

Goldstein, P. and Snoker, A. SAC availability for the IRIS community. *IRIS Data Management Center Electronic Newsletter*, <https://ds.iris.edu/ds/newsletter/>, 2005.

Goldstein, P., Dodge, D., Firpo, M., and Minner, L. SAC2000: Signal processing and analysis tools for seismologists and engineers. The IASPEI International Handbook of Earthquake and Engineering Seismology, Acad. Press, London, ed. W.H.K. Lee, H. Kanamori, P.C. Jennings and C. Kisslinger, 2003.

Hall, R. and Spakman, W. Mantle structure and tectonic history of SE Asia. *Tectonophysics*, 658:14–45, Sept. 2015. doi: [10.1016/j.tecto.2015.07.003](https://doi.org/10.1016/j.tecto.2015.07.003).

Herrin, E. and Taggart, J. Source bias in epicenter determinations. *Bulletin of the Seismological Society of America*, 58(6): 1791–1796, Dec. 1968. doi: [10.1785/BSSA0580061791](https://doi.org/10.1785/BSSA0580061791).

International Seismological Centre. ISC-EHB dataset. <https://doi.org/10.31905/PY08W6S3>, 2020. doi: [10.31905/PY08W6S3](https://doi.org/10.31905/PY08W6S3).

Kennett, B. L. N., Engdahl, E. R., and Buland, R. Constraints on seismic velocities in the Earth from traveltimes. *Geophysical Journal International*, 122(1):108–124, July 1995. doi: [10.1111/j.1365-246X.1995.tb03540.x](https://doi.org/10.1111/j.1365-246X.1995.tb03540.x).

Lomax, A., Bagagli, M., Gaviano, S., Cianetti, S., Jozinović, D., Michelini, A., Zerafa, C., and Giunchi, C. Effects on a deep-learning, seismic arrival-time picker of domain-knowledge based preprocessing of input seismograms. *Seismica*, 3(1), June 2024. doi: [10.26443/seismica.v3i1.1164](https://doi.org/10.26443/seismica.v3i1.1164).

Motulsky, H. J. and Brown, R. E. Detecting outliers when fitting data with nonlinear regression - a new method based on robust nonlinear regression and the false discovery rate. *BMC bioinformatics*, 7:123, Mar. 2006. doi: [10.1186/1471-2105-7-123](https://doi.org/10.1186/1471-2105-7-123).

Mousavi, S. M., Sheng, Y., Zhu, W., and Beroza, G. C. STanford EArthquake Dataset (STEAD): A global dataset of seismic signals for AI. *IEEE Access*, 7:179464–179476, 2019. doi: [10.1109/ACCESS.2019.2947848](https://doi.org/10.1109/ACCESS.2019.2947848).

Naranjo, D., Parisi, L., Jónsson, S., Jousset, P., Werthmüller, D., and Weemstra, C. Ocean bottom seismometer clock correction using ambient seismic noise. *Seismica*, 3(1), Jan. 2024. doi: [10.26443/seismica.v3i1.367](https://doi.org/10.26443/seismica.v3i1.367).

Nolet, G. *A Breviary of Seismic Tomography*. Cambridge Univ. Press, Cambridge, U.K., 2008.

Nolet, G. MERMAID data processing tutorial. <https://www.geoazur.fr/GLOBALSEIS/nolet/allpubs.html>, 2024.

Nolet, G. and van der Lee, S. Error estimates for seismic body wave delay times in the ISC-EHB Bulletin. *Geophysical Journal International*, 231(3):1739–1749, Sept. 2022. doi: [10.1093/gji/gac282](https://doi.org/10.1093/gji/gac282).

Nolet, G., Simon, J. D., and Bonnieux, S. How accurately are MERMAID seismograms located? *Seismological Research Letters*, 95 (4):2368–2374, Mar. 2024. doi: [10.1785/0220230377](https://doi.org/10.1785/0220230377).

Pasyanos, M. E., Masters, T. G., Laske, G., and Ma, Z. LITHO1.0: An updated crust and lithospheric model of the Earth. *Journal of Geophysical Research: Solid Earth*, 119(3):2153–2173, 2014. doi: [10.1002/2013JB010626](https://doi.org/10.1002/2013JB010626).

Pipatprathanporn, S. and Simons, F. J. Waveform modelling of hydroacoustic teleseismic earthquake records from autonomous MERMAID floats. *Geophysical Journal International*, 239(1): 136–154, Oct. 2024. doi: [10.1093/gji/ggaae238](https://doi.org/10.1093/gji/ggaae238).

Rösler, B., Stein, S., and Spencer, B. When are non-double-couple components of seismic moment tensors reliable? *Seismica*, 2 (1), Mar. 2023. doi: [10.26443/seismica.v2i1.241](https://doi.org/10.26443/seismica.v2i1.241).

Rösler, B., Stein, S., Ringler, A., and Vackář, J. Apparent non-double-couple components as artifacts of moment tensor inversion. *Seismica*, 3(1), Apr. 2024. doi: [10.26443/seismica.v3i1.1157](https://doi.org/10.26443/seismica.v3i1.1157).

Sepúlveda, I., Tozer, B., Haase, J. S., Liu, P. L., and Grigoriu, M. Modeling uncertainties of bathymetry predicted with satellite altimetry data and application to tsunami hazard assessments. *Journal of Geophysical Research: Solid Earth*, 125(9): e2020JB019735, Sept. 2020. doi: [10.1029/2020JB019735](https://doi.org/10.1029/2020JB019735).

Simon, J. D., Simons, F. J., and Nolet, G. Multiscale estimation of event arrival times and their uncertainties in hydroacoustic records from autonomous oceanic floats. *Bulletin of the Seismological Society of America*, 110(3):970–997, June 2020. doi: [10.1785/0120190173](https://doi.org/10.1785/0120190173).

Simon, J. D., Simons, F. J., and Irving, J. C. E. Recording earthquakes for tomographic imaging of the mantle beneath the South Pacific by autonomous MERMAID floats. *Geophysical Journal International*, 228(1):147–170, Sept. 2021. doi: [10.1093/gji/ggab271](https://doi.org/10.1093/gji/ggab271).

Simons, F. J., Nolet, G., Georgief, P., Babcock, J. M., Regier, L. A., and Davis, R. E. On the potential of recording earthquakes for global seismic tomography by low-cost autonomous instruments in the oceans. *Journal of Geophysical Research: Solid Earth*, 114 (B5):2008JB006088, May 2009. doi: [10.1029/2008JB006088](https://doi.org/10.1029/2008JB006088).

Sukhovich, A., Irisson, J.-O., Simons, F. J., Ogé, A., Hello, Y., Deschamps, A., and Nolet, G. Automatic discrimination of underwater acoustic signals generated by teleseismic P-waves: A probabilistic approach. *Geophysical Research Letters*, 38(18): 6469–6485, Sept. 2011. doi: [10.1029/2011GL048474](https://doi.org/10.1029/2011GL048474).

Vallée, M. and Douet, V. A new database of source time functions (STFs) extracted from the SCARDEC method. *Physics of the Earth and Planetary Interiors*, 257:149–157, Aug. 2016. doi: [10.1016/j.pepi.2016.05.012](https://doi.org/10.1016/j.pepi.2016.05.012).

Vallée, M., Charléty, J., Ferreira, A. M. G., Delouis, B., and Vergoz, J. SCARDEC: a new technique for the rapid determination of seismic moment magnitude, focal mechanism and source time functions for large earthquakes using body-wave deconvolution: Wave deconvolution and earthquake parameters. *Geophysical Journal International*, 184(1):338–358, Jan. 2011. doi: [10.1111/j.1365-246X.2010.04836.x](https://doi.org/10.1111/j.1365-246X.2010.04836.x).

Veronin, S., Mikesell, D., Slezak, I., and Nolet, G. Solving large tomographic linear systems: size reduction and error estimation. *Geophysical Journal International*, 199(1):276–285, Oct. 2014. doi: [10.1093/gji/ggu242](https://doi.org/10.1093/gji/ggu242).

Weatherall, P., Marks, K. M., Jakobsson, M., Schmitt, T., Tani, S., Arndt, J. E., Rovere, M., Chayes, D., Ferrini, V., and Wigley, R. A new digital bathymetric model of the world's oceans. *Earth and Space Science*, 2(8):331–345, Aug. 2015. doi: [10.1002/2015EA000107](https://doi.org/10.1002/2015EA000107).

Wessel, P., Luis, J. F., Uieda, L., Scharroo, R., Wobbe, F., Smith, W. H. F., and Tian, D. The generic mapping tools version 6. *Geochemistry, Geophysics, Geosystems*, 20(11):5556–5564, Nov. 2019. doi: [10.1029/2019GC008515](https://doi.org/10.1029/2019GC008515).

Weston, J., Engdahl, E. R., Harris, J., Di Giacomo, D., and Storchak, D. A. ISC-EHB: reconstruction of a robust earthquake data set. *Geophysical Journal International*, 214(1):474–484, July 2018. doi: [10.1093/gji/ggy155](https://doi.org/10.1093/gji/ggy155).

The article *Picking first arrivals in hydroacoustic seismo-*

grams from MERMAID floats © 2025 by Guust Nolet is licensed under CC BY 4.0.